



HAL
open science

Tunability of the Free-Spectral Range by Microwave Injection into a Mid-Infrared Quantum Cascade Laser

Etienne Rodriguez, Alireza Mottaghizadeh, Djamal Gacemi, Mathieu Jeannin, Zahra Asghari, Angela Vasanelli, Yanko Todorov, Qi Jie Wang, Carlo Sirtori

► **To cite this version:**

Etienne Rodriguez, Alireza Mottaghizadeh, Djamal Gacemi, Mathieu Jeannin, Zahra Asghari, et al.. Tunability of the Free-Spectral Range by Microwave Injection into a Mid-Infrared Quantum Cascade Laser. *Laser and Photonics Reviews*, 2020, 14 (5), pp.1900389. 10.1002/lpor.201900389 . hal-02784728

HAL Id: hal-02784728

<https://hal.science/hal-02784728>

Submitted on 8 Mar 2024

HAL is a multi-disciplinary open access archive for the deposit and dissemination of scientific research documents, whether they are published or not. The documents may come from teaching and research institutions in France or abroad, or from public or private research centers.

L'archive ouverte pluridisciplinaire **HAL**, est destinée au dépôt et à la diffusion de documents scientifiques de niveau recherche, publiés ou non, émanant des établissements d'enseignement et de recherche français ou étrangers, des laboratoires publics ou privés.

Tunability of the free-spectral range by microwave injection into a mid-infrared quantum cascade laser

Rodriguez, Etienne; Mottaghizadeh, Alireza; Gacemi, Djamal; Jeannin, Mathieu; Asghari, Zahra; Vasanelli, Angela; Todorov, Yanko; Wang, Qi Jie; Sirtori, Carlo

2020

Rodriguez, E., Mottaghizadeh, A., Gacemi, D., Jeannin, M., Asghari, Z., Vasanelli, A., Todorov, Y., Wang, Q. J. & Sirtori, C. (2020). Tunability of the free-spectral range by microwave injection into a mid-infrared quantum cascade laser. *Laser and Photonics Reviews*, 14(5), 1900389-. <https://dx.doi.org/10.1002/lpor.201900389>

<https://hdl.handle.net/10356/147858>

<https://doi.org/10.1002/lpor.201900389>

© 2020 The Authors. Published by WILEY-VCH Verlag GmbH & Co. KGaA, Weinheim This is an open access article under the terms of the Creative Commons Attribution License, which permits use, distribution and reproduction in any medium, provided the original work is properly cited.

Downloaded on 08 Mar 2024 21:43:09 SGT

Tunability of the Free-Spectral Range by Microwave Injection into a Mid-Infrared Quantum Cascade Laser

Etienne Rodriguez,* Alireza Mottaghizadeh, Djamal Gacemi, Mathieu Jeannin, Zahra Asghari, Angela Vasanelli, Yanko Todorov, Qi Jie Wang,* and Carlo Sirtori*

The free-spectral range (FSR) of quantum cascade lasers (QCLs) emitting at 4.7 μm can be tuned through direct microwave modulation. The intrinsic short carrier lifetime of inter-subband transitions, along with impedance matched electrical packaging, allows a high-speed modulation up to more than 30 GHz. A significant broadening and flattening of the lasing spectrum is observed under radio frequency (RF) injection with frequencies close to the round-trip cavity. An accurate analysis of the high resolution spectra of the laser shows a comb-like regime for both free-running and RF modulated QCLs, if the modulation frequency is within the locking-range of the device. One of the main advantages of collecting high-resolution mid-infrared spectra, over the plain investigation of the beatnote in the microwave region, is the access to all the longitudinal modes and thus the accurate measure of the FSR over the whole optical spectrum. The use of high-resolution spectroscopy provides an in-depth and comprehensive analysis of lasing spectra under microwave modulations.

mechanism responsible for the self-comb formation in QCLs has becoming a promising research topic in this field.^[1,2] New techniques have been developed to study the phase and the stabilities of frequency comb QCL. The shifted-wave interference Fourier-transform spectroscopy (SWIFTS) measures the intermodal phase relation of the QCL comb using a coherent beatnote spectroscopy^[3] and the Fourier-transform analysis of comb emission (FACE) study of the dual-comb multi-heterodyne detection and Fourier-transform analysis.^[4] Both cases are consistent and show a non-trivial phase relation among the modes translating the complex mode-locking mechanism. Indeed, the strong dipole matrix elements of ISBT allow giant second and third order susceptibilities responsible for the generation of four-wave mixing (FWM) in QCLs.^[5-9]

1. Introduction


The development of quantum devices based on inter-subband transitions (ISBT), especially since the invention of quantum cascade lasers (QCLs), has revealed significant advantages in the mid-infrared (MIR) domain. In addition to their compactness and electrical pumping, the unique properties of QCLs offer a remarkable degree of freedom for the choice of the wavelength emission and, contrary to conventional laser, are suitable for high-speed applications due to their ultrashort carrier lifetime. Recently, the comprehension of the intrinsic nonlinear

FWM is a powerful mechanism for generating a stable frequency comb regime in the MIR region owing to its extremely broad bandwidth resulted from the ultrashort intrinsic lifetime of these quantum structures.^[8,10]

In the case of low-dispersion spectra, the common beating signal of the optical modes in the radio frequency (RF) domain induces a modulation of the population inversion which is converted into a resonance in the current through the structure. Conversely, an external direct microwave modulation at

Dr. E. Rodriguez, Prof. Q. J. Wang, Prof. C. Sirtori
School of Electrical and Electronic Engineering
Nanyang Technological University
Singapore 639798, Singapore
E-mail: etienne.rodriguez@phys.ens.fr; qjwang@ntu.edu.sg;
carlo.sirtori@ens.fr

Dr. E. Rodriguez, Prof. Q. J. Wang
CINTRA CNRS/NTU/THALES
UMI 3288
Research Techno Plaza
50 Nanyang Drive, Border Block, Level 6 Singapore 637553, Singapore
Dr. A. Mottaghizadeh, Dr. Z. Asghari
Laboratoire Matériaux et Phénomènes Quantiques
UMR7162
Université de Paris
Paris 75013, France
Dr. D. Gacemi, Dr. M. Jeannin, Prof. A. Vasanelli, Dr. Y. Todorov,
Prof. C. Sirtori
Laboratoire de Physique de l'Ecole Normale Supérieure
ENS
Université PSL
CNRS
Sorbonne Université
Université de Paris
24 rue Lhomond, Paris 75005, France

 The ORCID identification number(s) for the author(s) of this article can be found under <https://doi.org/10.1002/lpor.201900389>

© 2020 The Authors. Published by WILEY-VCH Verlag GmbH & Co. KGaA, Weinheim. This is an open access article under the terms of the Creative Commons Attribution License, which permits use, distribution and reproduction in any medium, provided the original work is properly cited.

DOI: 10.1002/lpor.201900389

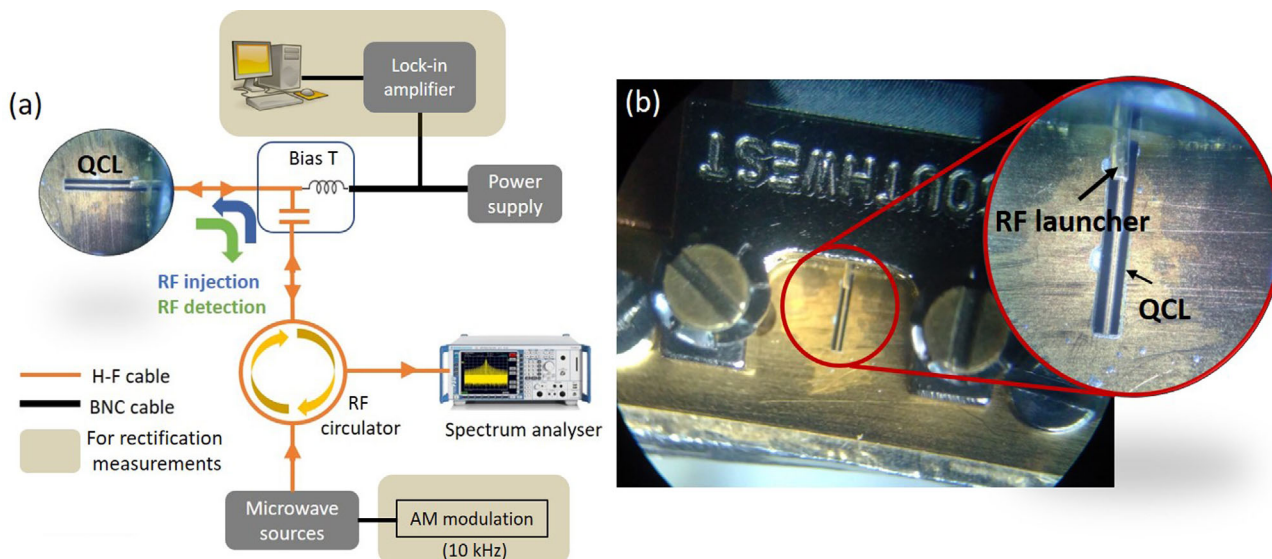


Figure 1. a) Setup used to inject and analyze the beating signal. The circulator and bias-T ensure the detection of the beatnote by the spectrum analyzer, and the injection of the microwave modulation in the device. The colored boxes represent the add-ons for the rectification measurements. b) Picture of the high-speed adaptation in the cryostat, the RF launcher is used to inject both AC and DC current in the QCL.

the round-trip frequency of the QCL can enhance this process and generates sidebands of the free-running modes. In the case of low-dispersion regions, it is known that active mode-locking through RF modulation can be achieved.^[10–12] Moreover, electrical injection-locking of MIR QCLs has been shown to be a powerful technique that enables the generation of coherent frequency combs along with the ability to mitigate the downside of the optical feedback which is an important obstacle to dual-comb spectroscopy based on QCLs.^[13,14] The abilities of operating QCLs at frequency comb regimes offer an opportunity for many breakthroughs in various areas. Coupled with the newly developed wide-band quantum well infrared photodetectors (QWIPs), they pave the way toward microwave optical links in the atmospheric window.^[15] For instance, recently, Pfeifle et al. have achieved a data transfer rate of 1.44 Tbit s⁻¹ over up to 300 km by using near-infrared frequency comb sources,^[16] demonstrating the capability of frequency comb in free-space communication applications. Besides, one of the great advances on dual-comb spectroscopy relies on their ability to tune the FSR to match narrow molecules absorption. Until now, this is mainly achieved by tuning the temperature or current of the QCL. The microwave injection permits an instantaneous shift of the FSR along with being a powerful tool for all-electrical frequency stabilization which would greatly benefit dual-comb multi-heterodyne experiments.^[13,17,18]

In this paper, we demonstrate high-speed modulation of QCLs emitting at 4.7 μm up to 30 GHz, the speed of which is limited by our RF generator. This high-speed behavior enables the amplitude modulation (AM) at the round-trip frequency of our QCLs. This external oscillator can interact with the beating signal, which corresponds to the free-spectral range (FSR) of the cavity, and allows injection pulling and injection-locking mechanisms. This interaction has been studied through the evolution of the high-resolution spectra for free-running and injection-locked QCLs. The free-running lasers display a multi-

mode operation with a narrow inter-mode beating signal. The external microwave modulation is injected at the same or a frequency close to the one of the beating signals, and we observe the injection-locking mechanism for a frequency placed at the locking-range of the beating signal. For both configurations, the high-resolution measurements show a constant FSR, corresponding to no observable dispersion beyond 10 MHz over the entire spectra. We also observed a noticeable generation of optical modes in the injection-locked spectra corresponding to sideband generation. Furthermore, these measurements allow us to observe clearly the change of the FSR following the frequency injected.

2. Sample Description and High-Speed Behavior

Recently, significant progress has been reported in the high-speed behavior of quantum devices based on ISBT, for instance, advanced design based on QCL embedded into microstrip line showed direct modulation up to 14 GHz.^[19] The lasers used in this article are standard buried-heterostructures of about 3 μm thick InGaAs/InAlAs active region grown on InP substrate by molecular-beam epitaxy at a emitting wavelength of 4.7 μm . Ridge lasers are processed with a width between 4 and 10 μm . The length of the cavity is of 2, 3, and 4 mm, which is directly related to the beating frequency. In order to improve the external modulation performance in the GHz range, the active region is embedded in a 70 μm thick, 50 Ω impedance matched microstrip waveguide as represented in the picture **Figure 1b** and illustrated in the inset of **Figure 2a**.

The high-speed behavior of continuous wave (CW) operated QCLs requires a specific configuration, for which the cryostat must be adapted for high-speed transmission. The analog current (AC) and direct current (DC) injection is done using an RF launcher that we carefully place on the ridge as seen in the inset

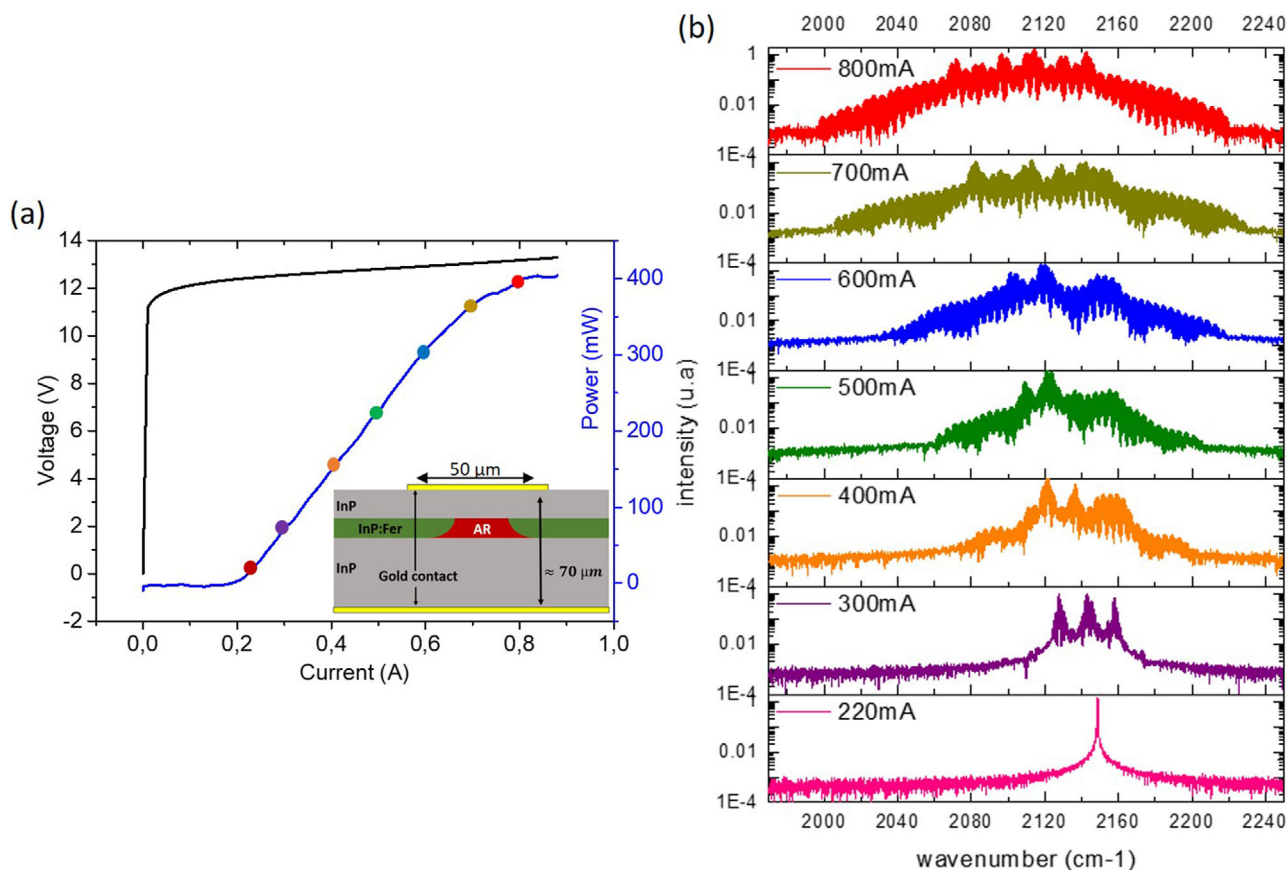


Figure 2. Characterization of the QCL used at CW operation at 80 K. a) current–voltage curves. The inset: diagram of the waveguide and b) spectra as a function of the current following the colored dots on the IV curve.

of Figure 1b. The packaging designed here would not be ideal in an environment with strong vibrations. To overcome this limitation an external coplanar waveguide can be attached to the ridge as a platform to weld the launcher. The electrical setup is shown in Figure 1a, where the RF circulator allows the injection and detection of the RF signal. We used a 45 GHz bias-T to ensure the DC and AC injection to the laser properly. The measurements of the current–voltage (IV) curves along with the RF injection and the detection of the modulated signal is ensured respectively by a source meter (KEITHLEY 2400), a signal generator (Anritsu MG3693B) and a spectrum analyzer (Agilent E4407B). The high-resolution spectrum was recorded using a Bruker IFS 125 HR Fourier transform infrared spectrometer (FTIR) at the AILES beamline of SOLEIL with an absolute resolution of 60 MHz. The more important parameters are the relative precision of the optical mode position, the implementation of zero-padding, and cubic spline interpolation which largely increase the peak precision and allow us to record spectra with a peak precision of about 6 MHz.

Figure 2a shows the IV characteristic of a 3 mm long and 10 μm wide QCL emitting at 4.7 μm and operating in CW at 80 K. Emission spectra are recorded at various pumping currents (at each dot along the IV curve) and reported in Figure 2b. The laser operates in single-mode near the threshold, and then a multimode behavior with the increase of the current with broadened

emission spectra spreading over more than 200 cm^{-1} near the roll-over.

The frequency response of the QCL is the product of the intrinsic transfer function of the laser, $h(\omega)$, and the transfer function of the electrical packaging.^[10] QCLs can be modeled as equivalent lumped element circuits acting as a low-pass filter. In standard designs, the inductance introduced by the wire bonding dominates the circuit response and decreases drastically the cut-off frequency of the circuit. **Figure 3a** shows the simulation for a gold wire bonding connecting the laser to a lossless RF injection line. The deep and light blue curves represent respectively the cut-off frequency for a single 3 and 1 mm gold wire. Therefore, to ensure high-frequency propagation, the wire bonding connection is replaced by the RF launcher placed on the top contact. As a consequence, the inductance can be neglected, and the electrical circuit becomes a simple RC circuit. The cut-off frequency of the packaging circuit only depends on the differential resistance and the equivalent capacitance of the active region and the insulator layer. The differential resistance depends on the injected current and the capacitance can be calculated using the parallel plate capacitor approximation. The black curve in Figure 3a displays the cut-off frequency of our device with a differential resistance of 2 Ω while the red curve corresponds to the capacitance introduced by the active region as a function of the surface of the active region for the different widths.

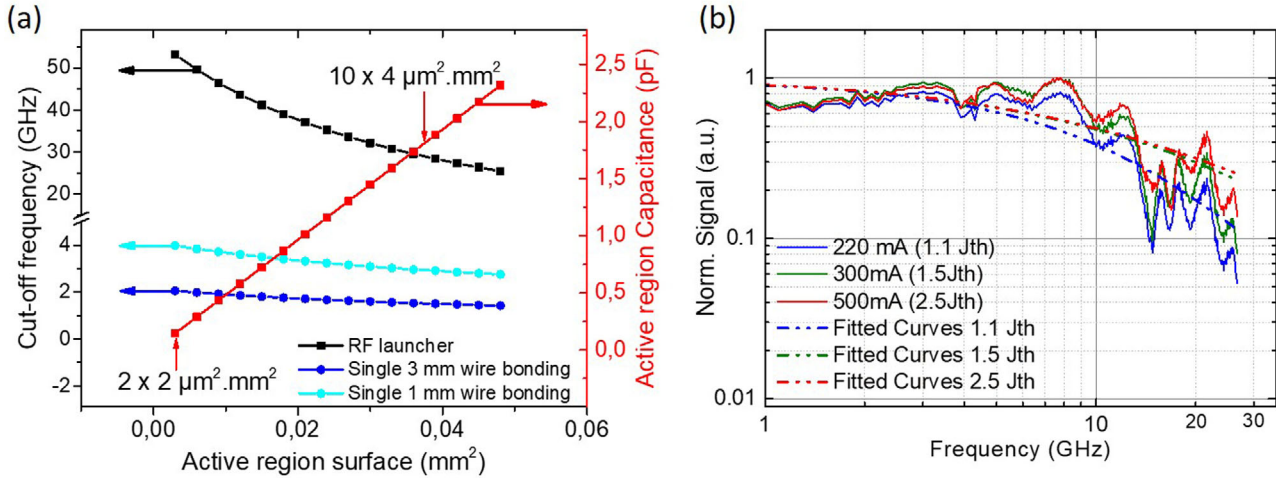


Figure 3. High-speed characterization of the QCL used at CW operation at 80 K. a) Capacitance of the active region of our laser (solid red line) and cut-off frequency for RF launcher (solid black line), single 3 and 1 mm wire bonding configurations (respectively solid deep and light blue line) as a function of the surface for a differential resistance of 2 Ω , and b) normalized rectification curves (solid line) and simulated curves (dashed line) for different J/J_{th} ratio up to 27 GHz.

The transient behavior and the theoretical frequency response of our quantum devices to a small modulation of the driving current can be expressed as^[10]

$$|h(\omega)| = \frac{1}{\sqrt{1 + \omega^4 \tau_{\text{phot}}^2 \tau_{\text{stim}}^2 + \omega^2 \tau_{\text{phot}} \tau_{\text{stim}} \left(\frac{\tau_{\text{phot}} \tau_{\text{stim}}}{\tau_3^2} + \frac{\tau_{\text{phot}}}{\tau_{\text{stim}}} + 2 \frac{\tau_{\text{phot}}}{\tau_3} - 2 \right)}}$$

$$\text{with } \tau_{\text{phot}} = \frac{n_{\text{eff}}}{c\alpha_{\text{tot}}} \text{ and } \tau_{\text{stim}}^{-1} = \left(\frac{J}{J_{th}} - 1 \right) \tau_3^{-1} \quad (1)$$

τ_{phot} represents the lifetime of the photon in the cavity which is inversely proportional to the total loss in the cavity, τ_{stim} the lifetime of the stimulated emission directly linked to the structure alignment before the gain saturation and τ_3 the upper state lifetime. For a QCL in the MIR region, the typical value of the upper state lifetime at low temperature is about one to few picoseconds.

The high-speed behavior of our devices is measured by the microwave rectification technique at 80 K. This technique exploits the inherent nonlinear IV characteristics of QCLs to investigate their frequency response by applying an RF signal to the QCL and measuring the variation of its DC biasing current. The rectification methods reflect the frequency roll-off behavior of the intrinsic transfer function and the electrical circuit, along with other parasitic effects.^[20,21] As shown in the colored boxes of Figure 1a, we applied an AM low-frequency modulation (10 kHz) to the RF generator and measure the DC rectification-voltage by the lock-in amplifier triggered at the frequency of the AM modulation. The variation of the current is then normalized and plotted on a log-scale graph for different driving currents. We used a RF injection power of 10 dBm with a step frequency of 100 MHz. The noise of the measurements was reduced by using a lock-in amplifier. Figure 3b exhibits the normalized rectification measurements performed at several J/J_{th} ratios in solid line limited by the RF generator which has a bandwidth of 30 GHz. The dashed line represents the simulation of the theoretical frequency response of the QCLs at the different currents considering the electrical

circuit and the different lifetimes. After the threshold, the differential resistance drops to about 2 Ω and the capacitance of the device calculated is ≈ 2 pF. The lifetime of the stimulated emission represents, for a current of 1.1, 2, and 2.5 J_{th} , a value of 10, 1, and 0.67 ps, while the photon lifetime is set at $\tau_{\text{phot}} = 6.6$ ps which corresponds to a loss of about 15 cm^{-1} . As described by the theory, before gain saturation the cut-off frequency increases with the J/J_{th} ratio, as it can be observed in Figure 3b. The electrical resonances observed around 15 GHz, corresponding to a centimeter scale, are not inherent to the devices and are due to the reflections in the electrical circuit, these artifacts are often experimentally observed.^[22,23]

The unique properties of ISBT, along with an impedance matched electrical circuit allow reaching a frequency modulation higher than 30 GHz. Therefore, this system unlocks all the benefits of an external modulation of the laser at the beating signal and opens the door to investigate the effect of an injection at the higher harmonics of the beating signal.

The high-speed behavior of our devices allows us to inject efficiently an external modulation at the FSR of our laser and generate new optical modes in the spectrum. The injection-locking mechanism of the beating signal is ease in low-dispersive regimes. However, in QCLs zero dispersion is not always required. The FWM process taking place in the active region is sensitive to the frequency and the relative phases of the optical modes. In low dispersion regime, it has the abilities to correct the dispersion by fixing the intermodal spacing and, therefore, facilitate the creation of frequency comb spectra. The material dispersion introduced by the InP and other materials constituting the waveguide is very low in the MIR (from 3.3 to 10 μm).^[24] The evolution of the electric field of the fundamental mode with the frequency, seen in the inset of Figure 4, introduces a change of the confinement factor which translates in a variation of the group refractive index of the longitudinal modes over the spectrum. Thus, as shown in Figure 4, the group velocity dispersion (GVD) decreases rapidly with the width of the ridge. Nevertheless, the expansion of the active region will lead to the appearance

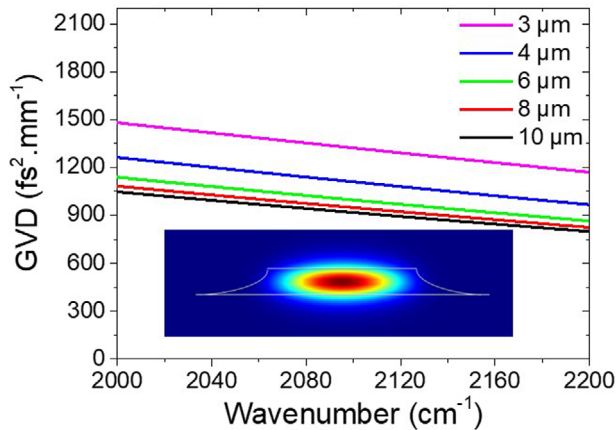


Figure 4. Waveguide dispersion for different widths of the ridges as a function of the wavenumber. Inset: simulation of the electric field of the fundamental mode in the waveguide.

of higher-order transverse modes oscillating in the Fabry–Perot (FP) cavity. As it is essential to maintain a low-dispersion regime to ensure frequency combs operation, a trade-off must be found between the dispersion management and the number of transverse modes lasing in the cavity.

To limit the waveguide dispersion of our devices, we will favor the use of wider active regions. For instance, for a waveguide of about 10 μm width without considering the contribution from the active region gain, the sum of the waveguide and material dispersion remains relatively low for a QCL in the MWIR.^[24] However, such large waveguide sustains higher-order transverse modes that may oscillate in the cavity and can perturb the high-resolution spectra analysis as observed in the measurements.

3. Injection-Locking and Results on the Optical Spectrum

The phenomenon of injection-locking is well described by Adler’s equation on coupled oscillators.^[25] Indeed, this phenomenon can be related to the locking injection between a master oscillator (here the microwave modulation) and the slave oscillator (here beating signal of the Fabry–Perot modes) such as

$$\Delta\omega_{\text{lock}} = \frac{2\omega_0}{Q} \sqrt{\frac{I_0}{I_1}} \quad (2)$$

Where ω_0 and I_0 represent respectively, the frequency and intensity of the microwave modulation, I_1 the intensity of the beating signal and Q the quality factor of the slave laser resonator. For an injected frequency highly detuned from the cavity frequency, the beating signal is unperturbed by the RF injection. When the RF frequency approached the round-trip frequency of the cavity, we observe the generation of RF sidebands and the pulling effect of the beatnote toward the injected frequency. While further increasing the frequency of the master oscillator, the beating signal gets fully injected and follows the frequency of the external microwave modulation within the locking-range. These observa-

tions are directly accessible in the RF domain. However, it is the same mechanism governing the injection locking in the spectral domain. The external modulation applied to the laser will create sideband separated by the injection frequency next to the Fabry–Perot cavity modes. When the sidebands are close enough to the next optical modes, the Fabry–Perot modes become locked to the master oscillator.^[19] As mentioned earlier, for free-running QCLs, the FWM is a passive mechanism. Nevertheless, it can be enhanced by an external microwave modulation at the same frequency than the beating signal. Thus, it can significantly broaden the spectrum by generating sidebands spaced by the injection frequency. On the other hand, for an injection out of the locking-range, the creation of the sidebands in the optical spectrum is too distant from the corresponding FP modes; they cannot be amplified by the gain and does not contribute to the evolution of the optical spectrum. Therefore, in the low-dispersion regions, the external microwave modulation at the round-trip frequency will not only generate new frequencies but also create a comb-like regime with a fixed spacing between the modes. **Figure 5a** shows the evolution of the spectrum with the power of the microwave modulation at the round-trip cavity of 4 mm emitting at 4.7 μm . We observed the generation of a large number of optical modes and a new distribution of the energy among them over the spectra. The sidebands generated are locked at the frequency of the RF generator which is at the round-trip frequency. This extends from about 25 cm^{-1} without injection to 54 cm^{-1} with 30 dBm injection. This extension is represented by the green area on the spectra with as boundaries the red dashed lines. Above the injection of 20 dBm (100 mW) the generation of new modes slows down, but we still observe a redistribution of energy between the modes. The FWM mechanism conducts to a broadening of the spectrum and the creation of a more homogeneous distribution of the amplitude among the modes. We studied this effect with a peak detection threshold within an amplitude of at least 1% and 10% of the maximum power of the optical peaks. **Figure 5b** records the increase of the number of modes as a function of the injected power. We define the total number of modes as the number of modes within an amplitude greater than 1% of the maximum amplitude. This quantity goes from about 25, without injection, to more than 120 for an injection at 30 dBm. The inset represents the percentage of modes within an amplitude of 90% of the highest peak, the proportion of peaks included in this ranges goes from 20% without injection to 60% of the optical modes with the RF injection. **Figure 5c** is a zoom-in, in linear scale, on the sideband generation between the free-running spectrum and the 0 dBm injection at the round-trip frequency. The net increase of number of longitudinal modes at low injected power corresponds to the redistribution of the energy of the principal cavity modes on their neighboring modes through the generation of sidebands, represented with different colors in the red spectrum. The relatively low overlap between the microwave mode and the active region and the high impedance mismatch between the source and the laser leads to an injection efficiency expected in the order of a few percent. Therefore, the observed effects on the spectra are generated with an injection power in the order of few tens of μW only. Due to the square roots dependence of the locking-range with the injected power, the optimization of the injection efficiency is crucial to achieving wider tunability of the FSR.

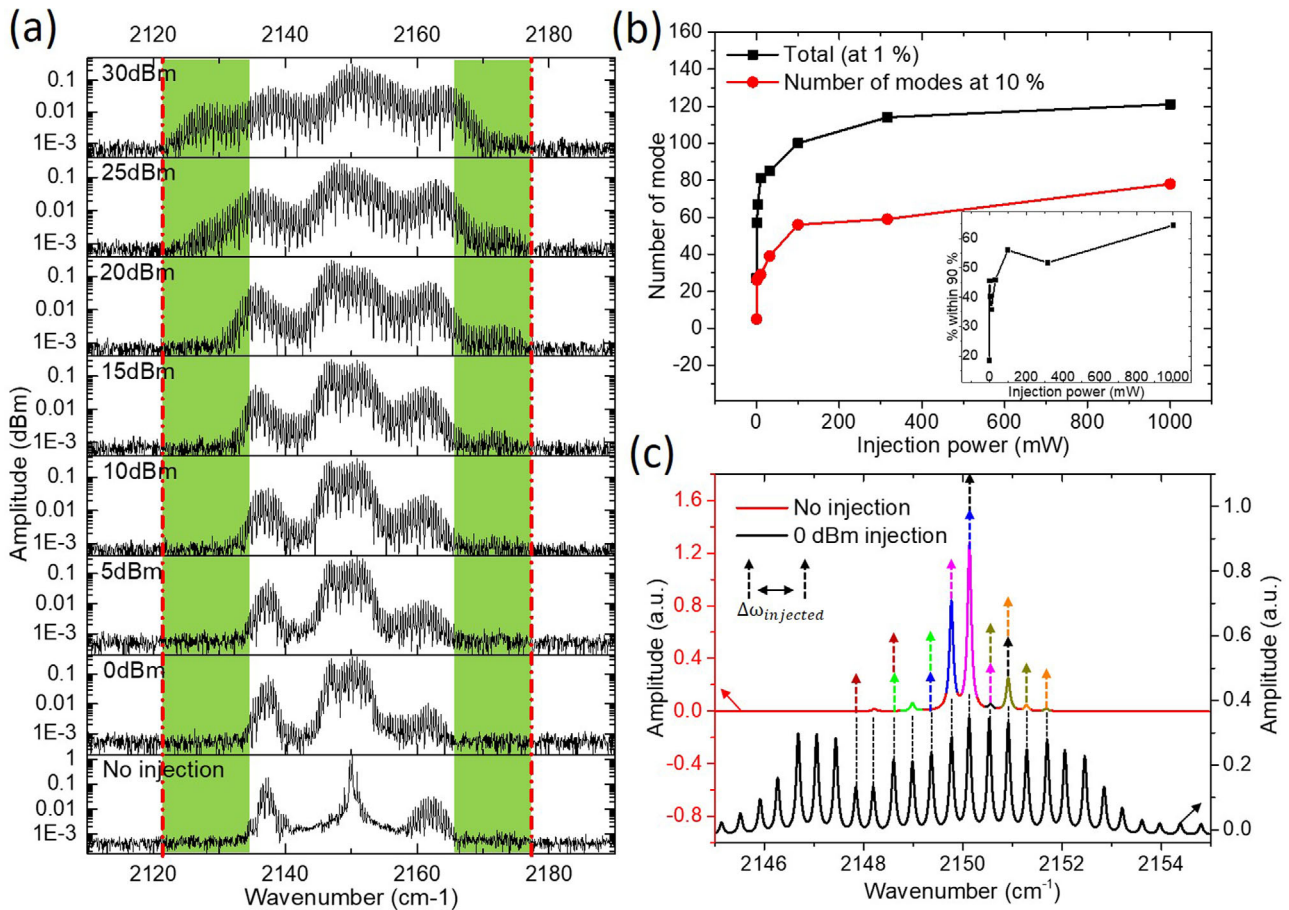


Figure 5. a) Evolution of the spectrum for several power injections for a 4 mm QCL at 4.7 μm with a current of 300 mA corresponding to 1.6 J_{th} ; b) evolution of the number of optical modes for different injected power. The red curve is the number of optical modes with an amplitude of at least 10% of the maximum power and the black curve corresponds to an amplitude of at least 1%. The inset represents the percentage of the modes included in an amplitude of 90% of the highest peak. c) Evolution of the high-intensity group of modes under 0 dBm injection. The dashed arrow illustrates the sidebands generation.

As the FWM is a frequency and phase sensitive process, this configuration has the potential to stabilize the frequency and phase of the modes generated.

The new generation of modes through the FWM process does not only have the ability to broaden the spectrum but also to compensate the dispersion. Indeed, the position of the new modes generated is placed at a frequency span described by the FSR, i.e., exactly positioned as a comb spectrum. They are acting as a master oscillator and, in the case of a low-dispersion regime, will lock the existing dispersed-modes. In that sense, if the dispersion remains small enough, the modes stay efficiently coupled by the FWM and act as a comb operation.^[24]

4. High-Resolution Study of the FSR

Each spectrum is recorded after the stabilization of the temperature. The parameters of the FTIR are set to achieve the highest resolution of the instrument described in the introduction. The acquisition time of the high-resolution spectra presented in the next studies was ≈ 20 min. No stabilization of the offset frequency was used for the measurements. The analyses of the single comb tooth for the high-resolution spectra show a Gaussian linewidth

whose half width at half maximum is $\approx 5 \times 10^{-3} \text{ cm}^{-1}$ (150 MHz). We do not observe an eventual frequency shift due to the current and temperature instabilities; moreover, the potential broadening of the FP modes due to these sources of noise would not influence the main results which are the peak frequencies of the modes.

The maximum of each optical mode is compared to the position of the previous and next modes, yielding the evolution of the FSR as a function of the mode number, or frequency. Since the FSR is related to the dispersion through the group refractive index n_g , a zero dispersion leads to a constant $n_g(\omega)$ and hence, a constant FSR. However, in the case of a nonzero dispersion, the peak position of each mode will be slightly shifted accordingly to the variation of the group refractive index and therefore, will introduce a frequency dependence of the FSR.

As described earlier, the wide waveguide used to reduce the dispersion allows the propagation of higher-order transverse modes with much lower intensities. Due to the finite resolution of the FTIR, the overlap between the fundamental and the high-order transverse modes of the cavity can result in a broadening of the comb tooth and therefore, an error in the peak frequency measurement. This phenomenon leads to a slight shift in the

position of the maximum of the fundamental mode which produces an unwanted variation of the FSR.

This is usually observed at the edge of the spectra where the cavity modes have comparable amplitudes. This phenomenon has also been observed in other experiments.^[26]

The use of high-resolution spectra allows us to see the dispersion into the MHz range and, therefore, reveals much more information than the basic observation of the beating signal. For instance, we can have a clear idea of the modes efficiently injected by the external modulation and master their FSR over a relatively large frequency span. **Figure 6a** is a zoom-in of the high-resolution spectra without injected (in gray) and with an injection at one of the extremities of the locking-range (in red). The upper part of **Figure 6b–d** represent the study of the FSR as a function of the wavenumber, while the lower part is the corresponding spectrum. The spectra are recorded for the QCL at a current of 400 mA with and without microwave modulation. An averaging is applied to the values of the FSR to smooth the oscillation due to the resolution. The red and green dashed lines and the yellow regions represent respectively, the frequency injected, the extremities of the locking-range and a frequency area of 10 MHz corresponding to approximately the resolution of the instrument. **Figure 6b** is the free-running spectrum without RF injection. **Figure 6c,d** represents a microwave modulation at 27 dBm for an injection in (red spectrum: M4) and out (green spectrum: M3) of the locking-range. We do not observe a variation of the modes spacing in the resolution of the FTIR, i.e., below 10 MHz. Nevertheless, the injection at the frequency 13 MHz lower than the beating signal is out of the locking-range (M3). In this case, only the small part of the spectrum indicated by the yellow region and the red dashed line is locked and follows the new FSR dictated by the microwave modulation. The next 70 modes are not locked and oscillate around a value following the not injected beatnote. The colored stars of **Figure 6e** displays the injection frequency (right axis) as a function of the average FSR measured over a stable area of the spectrum. The left axis corresponds to the colored histograms of the repartition of the FSR over the spectrum for each measurement (M2, M3, M4, and M5). The different microwave injections in the RF domain are represented in **Figure 7a**. The yellow area illustrates the locking-range of the laser at this injection power. For an RF injection detuned from the beating signal, we can observe the shift of the FSR correspondingly. Each bin size represents a frequency window of 6 MHz. As seen previously, for a microwave modulation in the locking-range, the FSR remains concentrated in the resolution. Nevertheless, for the measurements M3, out of the locking-range, we observe a significant broadening represented on the green histogram.

With or without injection in the locking-range, the high-resolution measurements do not show any dispersion within the resolution of the FTIR. Therefore, we can conclude that more than 90% of the optical power produced by the laser has a constant FSR within 10 MHz. Regardless of the thin beating signal of the free-running modes, the analysis of the mode spacing shows a frequency comb-like regime^[2], for the free-running and injection-locked QCL. Nevertheless, a phase analysis of the modes is required to claim a frequency comb regime.

Similar measurements have been realized at different current densities and on QCLs emitting at 9 μm and draw the same conclusion.

5. Tunability of the FSR

The constant FSR over the spectrum is an important tool for many applications. Adding to that, the potential to tune the FSR over a range of frequency offers a new degree of freedom which opens the door to strong advantages in several applications, especially in multi-heterodyne measurements and dual-comb spectroscopy. In this study, we will further investigate the tunability of the FSR of our QCLs presented in the previous paragraph under microwave modulation. **Figure 7a** illustrates the measurements in the RF domain, with in solid gray arrow the beating signal of the free-running laser and in dashed colored arrows the frequencies of the different injections in and out of the locking-range. Each measurement is noted as MX, with X the number of the measurement (M1 corresponds to the spectrum without injection). The change of the FSR is investigated for injection at each extremity of the locking-range (M5 and M4), on the beatnote (M2) and out of the locking-range (M3).

To study the tunability of the FSR under a microwave modulation we compare the position of the optical mode N_i of the injected spectra with the equivalent optical mode of the noninjected spectrum as illustrated in **Figure 7b**. The first mode (N_1) is chosen arbitrarily from the beginning of the free-running spectrum as a reference. In an ideal case, the frequency of the mode with respect to the first mode N_1 is given by $\omega_i = \omega_1 + i \times \text{FSR}$ with i an integer number. Upon RF injection, this relation translates to $\omega'_{i,\text{inj}} = \omega'_1 + i * \text{FSR}_{\text{inj}}$. ω_i and $\omega'_{i,\text{inj}}$ represent respectively the frequency of the i th mode for the free-running spectrum and the injected spectra. To simplified and remove the frequency offset we will shift all the injected spectra to the same first comb mode $\omega'_1 - \omega_1 = 0$. Hence, the shift between the injected and noninjected peak frequency, $\Delta\omega = \omega'_{i,\text{inj}} - \omega_i$, follows a linear relation given by $\Delta\omega = i \times (\text{FSR}_{\text{inj}} - \text{FSR})$. Consequently, the variation of the frequency shift between two consecutive modes is proportional to the mode number. This proportionality coefficient is simply the frequency difference between the injected and free-running beatnotes. **Figure 7c** displays the analysis of the variation of the peak position under RF injection compared to the reference value without injection (ΔMX). The injection at a frequency higher than the beating signals increase the value of the FSR (in cm^{-1}), and thus, exhibits a positive slope corresponding to the difference of frequency between the beatnote of the free-running QCL and the RF injection. On the contrary, the injection at a lower frequency will decrease the value of the FSR and introduce a negative slope. We can noticeably observe the evolution of the peak position which shows the adaptation of the modes to the microwave modulation over the entire spectrum. Regarding the injection out of the locking-range, as observed previously, only the first modes are locked to the injected frequency. The dashed line corresponds to the slope expected for the injection, i.e., the variation of the FSR with the not injected spectrum. These values, along with the experimental slopes are recorded in **Table 1**.

For the injection in the locking-range all the modes follow the expected slopes, it implies that they have been efficiently locked at the frequency of the microwave modulation. As observed previously, the higher-order transverse modes are generating the breaks of the slopes noticed at the beginning and end of the curves. **Table 1** lists the expected values of the slope

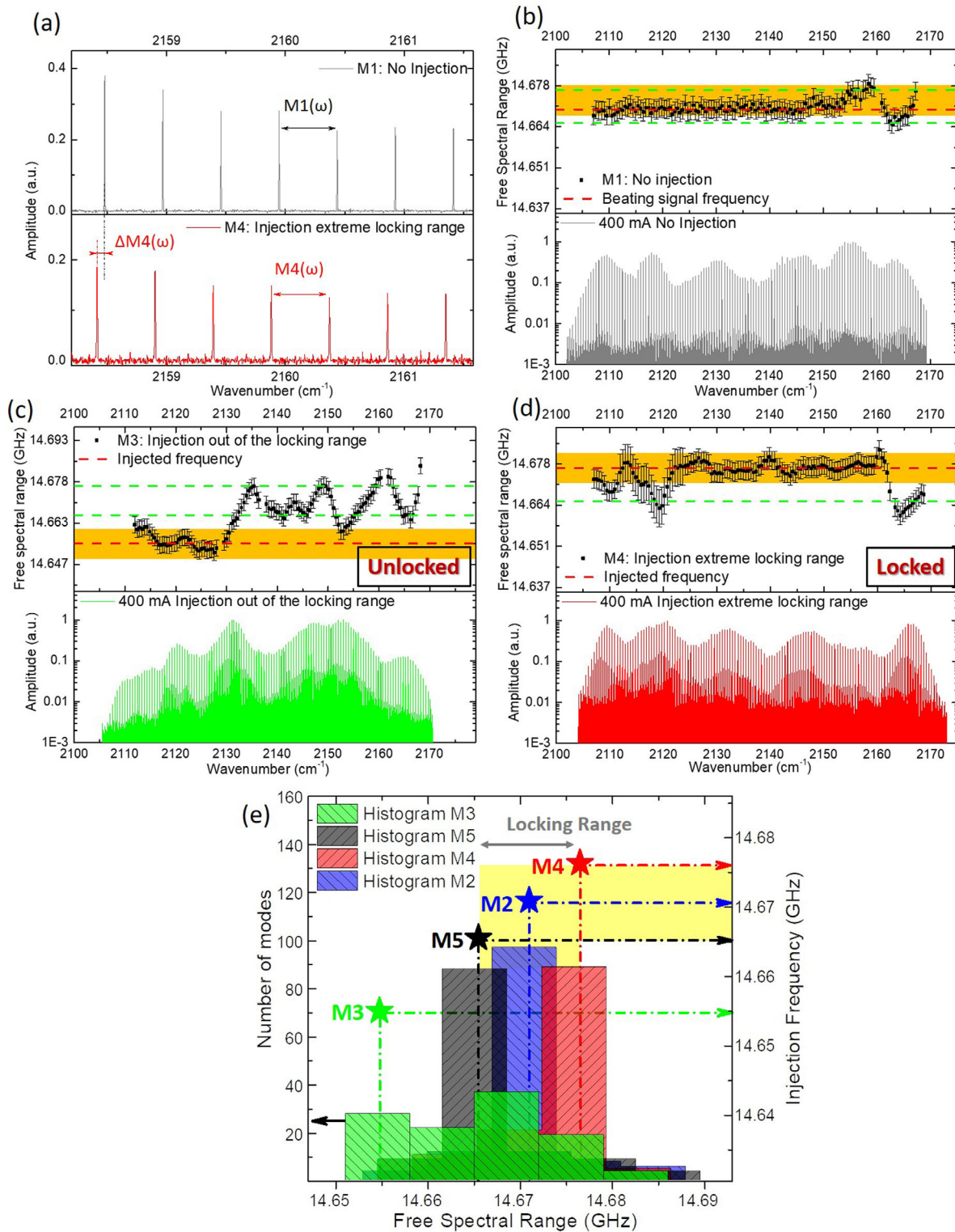


Figure 6. a) Zoom-in of the high-resolution spectra without injected (in gray) and with an injection at one of the extremities of the locking-range (in red). b–d) Analysis of the variation of the FSR over the spectra of a QCL emitting at $4.7 \mu\text{m}$ driven by a current of 400 mA with or without injection. The upper parts represent the FSR as a function of the wavenumber with the yellow region exhibiting a frequency area of 10 MHz and the lower parts showing the corresponding spectrum. b) The spectrum of the free-running QCL in gray, c,d) spectra with an RF injection, respectively, at the higher extremity of the locking-range in red and out of the locking-range in green. The injection frequencies and the extremities of the locking-range are indicated in dashed red and green lines. e) The right axis represents the injection frequency as a function of the average FSR measured over a stable area of the spectrum and the left axis is the histograms of the FSR repartition for each measurement. The yellow area represents the locking-range of the device.

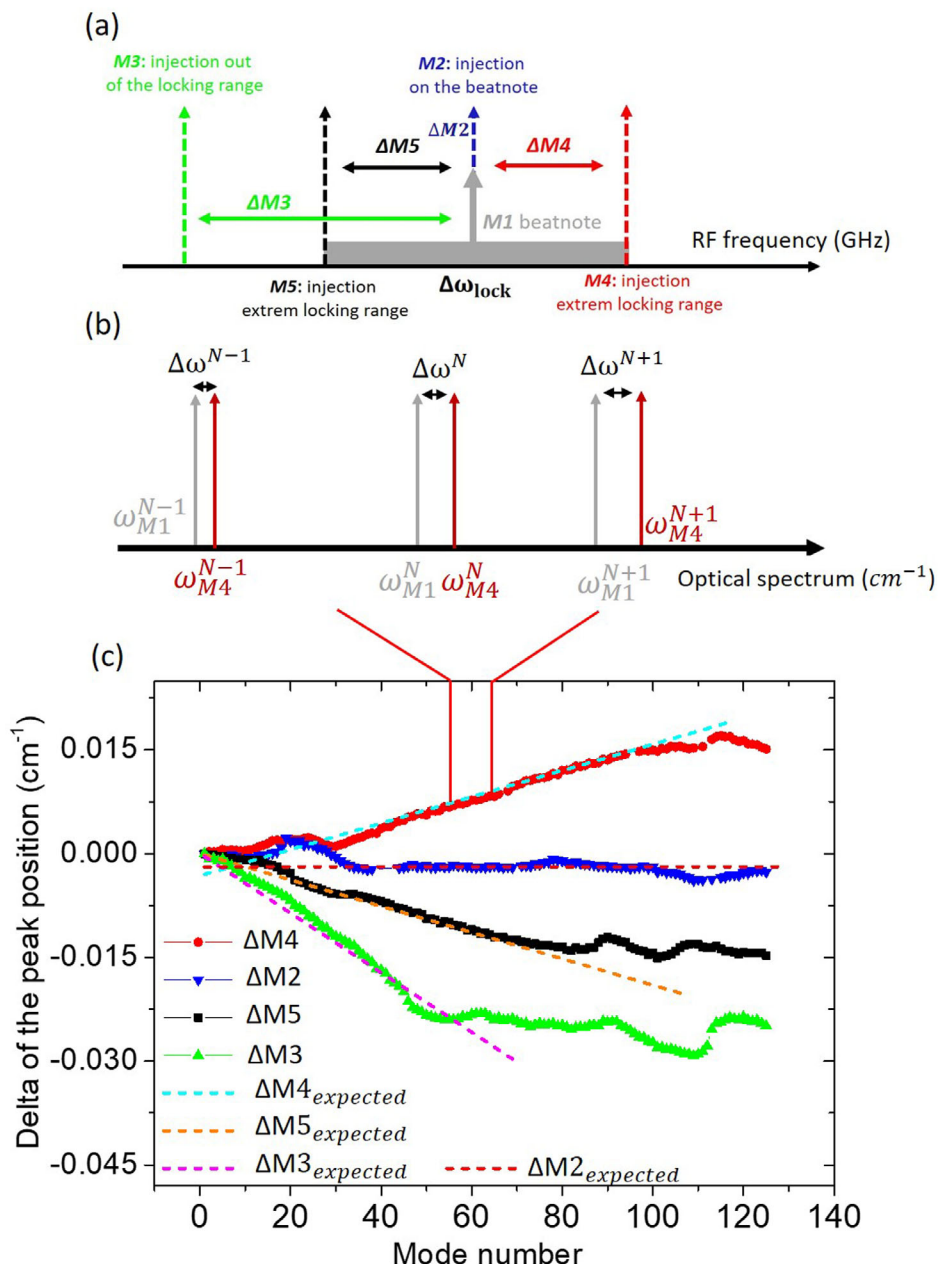


Figure 7. Measurements M1 without and M2, M3, M4, and M5 with RF injection at 27 dBm. a) Illustration of the measurement with RF injection at different frequencies in and out of the locking range represented in gray, b) representation of the variation $\Delta\omega$ of the peak position between the free-running spectrum (gray) and injected spectrum (red). c) The variation of the peak position between the spectra injected (M2, M3, M4, or M5) and the spectrum noninjected taken as reference (M1) with the expected slope in dashed line ($\Delta M2$, $\Delta M3$, $\Delta M4$, $\Delta M5$).

Table 1. Experimental and calculated values of the shift of the FSR under microwave modulation.

Measurements	Slope expected [cm^{-1}]	Real slope [cm^{-1}]
$\Delta M5$ (extreme low frequency of the range)	1.9×10^{-4} (5.7 MHz)	1.9×10^{-4} (5.6 MHz)
$\Delta M4$ (extreme high frequency of the range)	-1.9×10^{-4} (-5.7 MHz)	-2.0×10^{-4} (-6 MHz)
$\Delta M2$ (on the beatnote)	≈ 0 (0 MHz)	In the noise

corresponding to the ΔM_X in Figure 7c and the experimental values given by a linear fit over the stable part of the spectrum for the analysis concerned. For the injection in the locking-range the experimental values are in an excellent agreement with the expected values. Moreover, we record a locking-range covering a frequency span of 13 MHz which is, as far as we know, the wider locking-range reported in MIR region. These results are consistent with the literature where the injection-locking of a THz comb QCL detuned from the beating signal introduces a shift of the dual-comb

Received: November 13, 2019

Revised: March 11, 2020

Published online: April 6, 2020

multi-heterodyne frequencies in the MHz range.^[14] Regarding the injection out of the locking-range ($\Delta M3$), only a small portion of the spectrum is locked and follows the modulation. The slope expected (-4.3×10^{-4} (-12.8 MHz)) is in accordance with the experimental slope (-4.7×10^{-4} (-14.1 MHz)) calculated over the modes locked (50 first modes). The remaining part of the spectrum does not follow this slope and, as seen previously, are not injected.

The external microwave modulation enables to tune the FSR over the locking-range. Same results have been found for different positions in the IV curve, lasers length, and for QCLs emitting at 9 μm . Beyond the advantages that bring too many applications, the fine study of the spectrum under an injection detuned from the beating signal can give important information on the dispersion and the correction of dispersion introduced by the FWM.

6. Conclusion

In conclusion, we have demonstrated high-speed QCL embedded in a microstrip line with a modulation band up to 30 GHz at cryogenic temperature where the highest frequency is limited by our test equipment. The modulation of the population inversion at the round-trip cavity, along with a design allowing low-dispersion, enable the generation of a large number of optical modes and a more homogenous distribution of the amplitude among the modes over the spectra, through FWM mechanism. The high-resolution spectra analysis shows no variation of the FSR within the resolution of the FTIR, (6 MHz), thereafter, showing a comb-like regime for free-running and RF injected operation over the entire spectrum. Furthermore, comparing the high-resolution spectra under microwave injection with the free-running spectrum, allows us to observe that the great majority of the longitudinal optical modes are separated by a frequency dictated by the master oscillator, which corresponds to a tunability of the FSR over the beat note locking-range. The ability of QCL to work as a comb-like regime and to tune FSR by microwave modulation makes them very promising for many applications in the atmospheric windows in the MIR, especially in heterodyne, dual comb spectroscopy and free-space communications.

Acknowledgements

The authors acknowledge Olivier Piralı for its help during the measurements of the QCLs emitting at 4.7 μm at Synchrotron Source Optimis e de Lumi re d'nergie Interm diaire du LURE (SOLEIL). Moreover, the authors would like to thank Fridolin Kwabia-Tchana and Xavier Landsheere for the measurements of the QCLs emitting at 9 μm at Laboratoire Inter-Universitaire des Syst mes Atmosph rique (LISA). Furthermore, this work was supported by the Singapore National Research Foundation, Competitive Research Program (NRF-CRP18-2017-02) and Singapore Ministry of Education Tier 2 Program (MOE2016-T2-2-159).

Conflict of Interest

The authors declare no conflict of interest.

Keywords

injection locking, mid-infrared region, quantum devices, tunability of the free-spectral-range, ultrafast devices

- [1] G. Villares, J. Faist, *Opt. Express* **2015**, *23*, 1651.
- [2] A. Hugi, G. Villares, S. Blaser, H. C. Liu, J. Faist, *Nature* **2012**, *492*, 229.
- [3] M. Singleton, P. Jouy, M. Beck, J. Faist, *Optica* **2018**, *5*, 948.
- [4] F. Cappelli, L. Consolino, G. Campo, I. Galli, D. Mazzotti, A. Campa, M. Siciliani de Cumis, P. Cancio Pastor, R. Eramo, M. R sch, M. Beck, G. Scalari, J. Faist, P. De Natale, S. Bartalini, *Nat. Photonics* **2019**, *13*, 562.
- [5] F. Capasso, C. Sirtori, A. Y. Cho, *IEEE J. Quantum Electron.* **1994**, *30*, 1313.
- [6] D. Walrod, S. Y. Auyang, P. a. Wolff, M. Sugimoto, *Appl. Phys. Lett.* **1991**, *59*, 2932.
- [7] M. R. St-Jean, M. I. Amanti, A. Bismuto, M. Beck, J. Faist, C. Sirtori, *Opt. Express* **2017**, *25*, 1847.
- [8] P. Friedli, H. Sigg, B. Hinkov, A. Hugi, S. Riedi, M. Beck, J. Faist, *Appl. Phys. Lett.* **2013**, *102*, 222104.
- [9] Q. Y. Lu, M. Razeghi, S. Slivken, N. Bandyopadhyay, Y. Bai, W. J. Zhou, M. Chen, D. Heydari, A. Haddadi, R. McClintock, M. Amanti, C. Sirtori, *Appl. Phys. Lett.* **2015**, *106*, 1.
- [10] J. Faist, *Quantum Cascade Lasers*, Oxford University, Oxford **2013**.
- [11] H. Li, P. Laffaille, D. Gacemi, M. Apfel, C. Sirtori, J. Leonardon, G. Santarelli, M. R sch, G. Scalari, M. Beck, J. Faist, W. H nsel, R. Holzwarth, S. Barbieri, *Opt. Express* **2015**, *23*, 33270.
- [12] L. Kuznetsova, C. Y. Wang, V. M. Gkortsas, L. Diehl, F. X. K rtner, M. A. Belkin, A. Belyanin, X. Li, D. Ham, H. Schneider, H. C. Liu, F. Capasso, *Conf. Lasers Electro-Opt./Int. Quantum Electron. Conf.* **2009**, CMBB6.
- [13] J. Hillbrand, A. M. Andrews, H. Detz, G. Strasser, B. Schwarz, *Nat. Photonics* **2019**, *13*, 101.
- [14] L. Consolino, M. Nafa, F. Cappelli, K. Garrasi, F. P. Mezzapesa, L. Li, A. G. Davies, E. H. Linfield, M. S. Vitiello, P. De Natale, S. Bartalini, *Nat. Commun.* **2019**, *10*, 2938.
- [15] E. Rodriguez, A. Mottaghizadeh, D. Gacemi, D. Palaferri, Z. Asghari, M. Jeannin, A. Vasanelli, A. Bigioli, Y. Todorov, M. Beck, J. Faist, Q. J. Wang, C. Sirtori, *ACS Photonics* **2018**, *5*, 3689.
- [16] J. Pfeifle, V. Brasch, M. Laueremann, Y. Yu, D. Wegner, T. Herr, K. Hartinger, P. Schindler, J. Li, D. Hillerkuss, R. Schmogrow, C. Weimann, R. Holzwarth, W. Freude, J. Leuthold, T. J. Kippenberg, C. Koos, *Nat. Photonics* **2014**, *8*, 375.
- [17] G. Villares, A. Hugi, S. Blaser, J. Faist, *Nat. Commun.* **2014**, *5*, 5192.
- [18] Y. Wang, M. G. Soskind, W. Wang, G. Wysocki, *Appl. Phys. Lett.* **2014**, *104*, 031114.
- [19] M. R. St-Jean, M. I. Amanti, A. Bernard, A. Calvar, A. Bismuto, E. Gini, M. Beck, J. Faist, H. C. Liu, C. Sirtori, *Laser Photonics Rev.* **2014**, *8*, 443.
- [20] H. C. Liu, J. Li, M. Buchanan, Z. R. Wasilewski, *IEEE J. Quantum Electron.* **1996**, *32*, 1024.
- [21] H. Schneider, H. C. Liu, *Quantum Well Infrared Photodetectors*, Springer Series in Optical Sciences, Springer, Berlin **2007**.
- [22] B. Hinkov, A. Hugi, M. Beck, J. Faist, *Opt. Express* **2016**, *24*, 3294.
- [23] A. Calvar, M. I. Amanti, M. Renaudat St-Jean, S. Barbieri, A. Bismuto, E. Gini, M. Beck, J. Faist, C. Sirtori, *Appl. Phys. Lett.* **2013**, *102*, 1.
- [24] J. Faist, G. Villares, G. Scalari, M. R sch, C. Bonzon, A. Hugi, M. Beck, *Nanophotonics* **2016**, *5*, 272.
- [25] R. Adler, *Proc. IEEE* **1973**, *61*, 1380.
- [26] M. R sch, G. Scalari, M. Beck, J. Faist, *Nat. Photonics* **2015**, *9*, 42.